

Rogue wave spectra of the Kundu-Eckhaus equation

Cihan Bayındır*

Engineering Faculty, Işık University, İstanbul, Turkey

(Received 23 March 2016; published 15 June 2016)

In this paper we analyze the rogue wave spectra of the Kundu-Eckhaus equation (KEE). We compare our findings with their nonlinear Schrödinger equation (NLSE) analogs and show that the spectra of the individual rogue waves significantly differ from their NLSE analogs. A remarkable difference is the one-sided development of the triangular spectrum before the rogue wave becomes evident in time. Also we show that increasing the skewness of the rogue wave results in increased asymmetry in the triangular Fourier spectra. Additionally, the triangular spectra of the rogue waves of the KEE begin to develop at earlier stages of their development compared to their NLSE analogs, especially for larger skew angles. This feature may be used to enhance the early warning times of the rogue waves. However, we show that in a chaotic wave field with many spectral components the triangular spectra remain as the main attribute as a universal feature of the typical wave fields produced through modulation instability and characteristic features of the KEE's analytical rogue wave spectra may be suppressed in a realistic chaotic wave field.

DOI: [10.1103/PhysRevE.93.062215](https://doi.org/10.1103/PhysRevE.93.062215)

I. INTRODUCTION

Rogue (freak) waves may be detected by spectral analysis before they become evident in time [1,2]. Although some recent attempts have tried to measure the wave field directly in the spatial domain using efficient signal processing techniques [3], spectral analysis is still the main tool especially for ultrafast optic studies [4,5].

Exact rogue wave solutions of the different integrable systems differ significantly in shape [5]. Therefore, it is natural to expect that their spectral features, possible early detection mechanisms, and times may differ as well. In this work we show that the spectra of the individual rogue wave solutions of the Kundu-Eckhaus equation (KEE) differ significantly from those of the nonlinear Schrödinger equation (NLSE). Although the spectra of the individual rogue waves are significantly different, the rogue wave spectra of the chaotic wave fields have certain similarities to the NLSE case.

The KEE is one of the integrable extensions of the NLSE [6,7]. It contains extensions of terms of the standard cubic NLSE, namely, the quintic and Raman-effect nonlinear terms [8–10]. One of the different versions of the KEE can be written in the form

$$i\psi_t + \psi_{xx} + 2|\psi|^2\psi + \beta^2|\psi|^4\psi - 2\beta i(|\psi|^2)_x\psi = 0, \quad (1)$$

where ψ is the complex amplitude, x and t are the spatial and temporal variables, respectively, and i is the imaginary number [8]. The β parameter is a real constant and β^2 is the coefficient of the quintic nonlinear term. The last term of the KEE represents the Raman effect, which accounts for the self-frequency shift of the waves [8]. The KEE can adequately model the propagation of the ultrashort pulses in nonlinear and quantum optics, which can possibly be used to describe the optical properties of the femtosecond lasers and can be used in femtochemistry studies. Some extensions of the NLSE, similar to the form of the KEE, where quintic nonlinearity is not included but third-order dispersion and gain and loss terms

are included, are also used as models in the soliton-similariton laser studies [11].

Some analytical periodic and rational solutions of the KEE given in Eq. (1) exist in the literature [8,10]. The first-order rational solution of the KEE is given by

$$\psi_1 = \exp[i(-\beta x + (\beta^2 + 2)t)] \frac{L_1 + iJ_1}{M_1} \exp\left[i\beta \frac{K_1}{M_1}\right], \quad (2)$$

where

$$\begin{aligned} L_1 &= -4x^2 - 16\beta tx - 16(\beta^2 + 1)t^2 + 3, & J_1 &= 16t, \\ M_1 &= 4x^2 + 16\beta tx + 16(\beta^2 + 1)t^2 + 1, & & \\ K_1 &= 4x^3 + 16(\beta^2 + 1)t^2x + 9x + 16\beta(x^2 + 1)t. & & \end{aligned} \quad (3)$$

This solution and some other analytical solutions are given in [8–10]. This first-order rational rogue wave solution is basically a skewed Peregrine soliton of the NLSE. Setting the parameter $\beta = 0$, the KEE reduces to the cubic NLSE for which the rogue wave solutions become obvious and become the rational soliton solutions of the NLSE [12]. For the cubic NLSE, the first- and higher-order rational rogue wave solutions can be seen in [12]. Second- and higher-order rational solutions of the KEE and a hierarchy of obtaining those rational solutions based on Darboux transformations are presented in [8]. They are basically skewed rogue waves obtained by gauge transforming the rogue wave solutions of the cubic NLSE. For the sake of brevity, we are not repeating their explicit formulas here. For the details of their formulation the reader is referred to [8].

II. SPECTRA OF INDIVIDUAL ROGUE WAVES

In order to analyze the properties of the rogue wave spectra in a chaotic wave field, first we should analyze the spectra of the individual rogue wave solutions of the KEE. We obtain the spectra by the Fourier transform operation. Throughout this paper we denote by F the spectrum obtained by Fourier transforming the wave field $\psi(x, t)$ in the spatial variable x ,

*cihan.bayindir@isikun.edu.tr

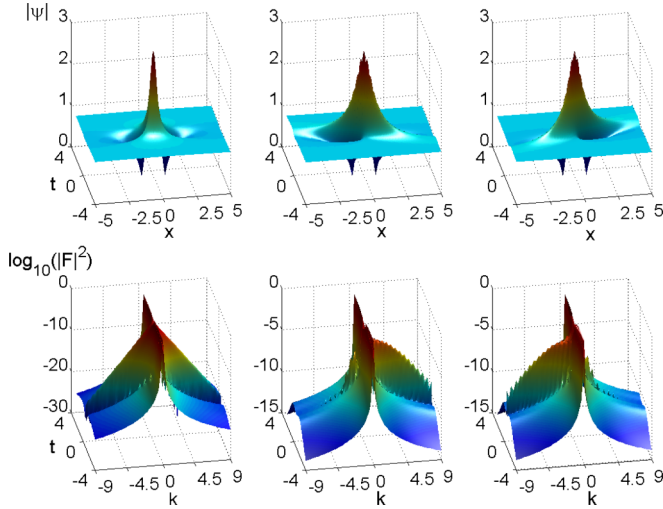


FIG. 1. The top row shows, from left to right, the first-order rogue wave of the KEE for $\beta = 0, 1,$ and $-1,$ respectively, and the bottom row shows the corresponding spectra on a logarithmic scale.

i.e.,

$$F(k,t) = \int_{-\infty}^{\infty} \psi(x,t) \exp(-ikx) dx, \quad (4)$$

where k denotes the wave-number parameter. The spectra calculated this way are complex functions and we present the energy spectral density $|F(k,t)|^2$ in all of the spectra calculations throughout this paper. The energy spectral density is a parameter that can be measured directly in experimental optics [5].

The first-order rational rogue wave solution of the KEE and the corresponding spectra are shown in Fig. 1 for $\beta = 0, 1, -1,$ respectively. The first three-dimensional (3D) plot in the bottom row of Fig. 1 shows the Fourier spectrum of the Peregrine soliton. The analytical form of this spectrum is given in [1] and for the sake of brevity it will not be repeated here. We compute the Fourier transform of the first-order rogue wave solution of the KEE given by Eq. (2) numerically by using fast Fourier transform routines. Three-dimensional plots of spectra of the first-order rational soliton solution of the KEE are also presented in the middle and right plots in the bottom row of Fig. 2 for $\beta = 1$ and $-1,$ respectively. The results depicted in Fig. 1 are also given as color contour plots in Fig. 2 for a better visualization of the spectra properties.

As discussed in [6,8], we can see that quintic and Raman-effect nonlinear terms produce an important skew angle relative to the ridge of the rogue waves. The sign of the β parameter determines the skewness direction relative to the ridge of the rogue wave [6,8]. If $\beta = 0,$ then there is no skewness and the rogue wave solution of the KEE reduces to the Peregrine soliton solution of the NLSE. For $\beta > 0,$ the skewness is in the counterclockwise direction, whereas for $\beta < 0$ it is in the clockwise direction [6,8]. Checking Figs. 2 and 3, the distinct feature of the rogue wave spectra of the KEE compared to their NLSE analogs is that the spectra are strongly asymmetric. For a skewness in the counterclockwise direction, which occurs due to the positive β parameter, the triangular widening occurs in the positive wave numbers.

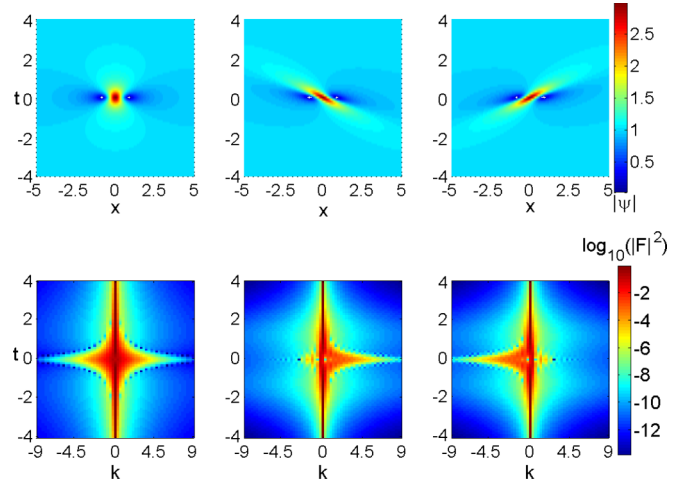


FIG. 2. The top row shows, from left to right, the color contour plot of the first-order rogue wave of the KEE for $\beta = 0, 1,$ and $-1,$ respectively, and the bottom row shows the color contour plot of the corresponding spectra on a logarithmic scale.

For negative values of the β parameter, this situation is reversed and triangular widening becomes apparent in the negative wave numbers. For both of the cases triangular widening is clearly distinguishable on only one side of the spectra.

Next we analyze the effect of increasing the skewness on the spectral features of the rogue waves of the KEE. For this purpose we set $\beta = 0, 1.75, -1.75$ and depict the corresponding spectra in Fig. 3. As can be seen from the contour plots given in Fig. 3, as the skewness of the rogue wave increases due to larger values of $|\beta|,$ the triangular widening of the spectra becomes more significant. Additionally, the asymmetry in the spectra becomes more prominent as well. For larger skewness, the higher absolute wave-number components begin to acquire some energy and they deviate from zero at earlier times of the rogue wave emergence compared to their NLSE analogs. For example, for $t \approx -5,$ the first-order rational solution of the

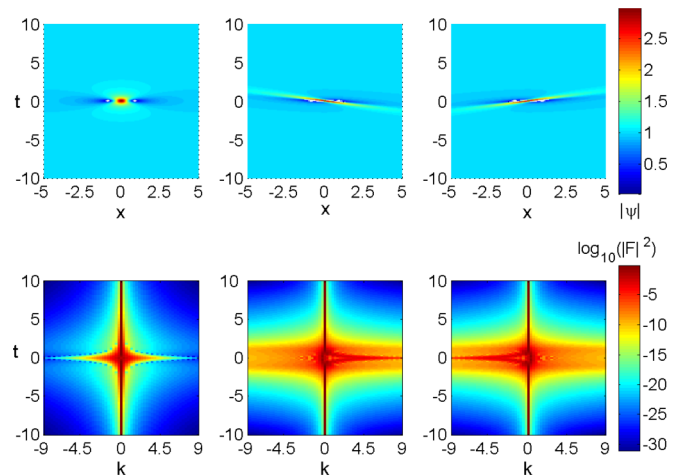


FIG. 3. The top row shows, from left to right, the color contour plot of the first-order rogue wave of the KEE for $\beta = 0, 1.75,$ and $-1.75,$ respectively, and the bottom row shows the color contour plot of the corresponding spectra on a logarithmic scale.

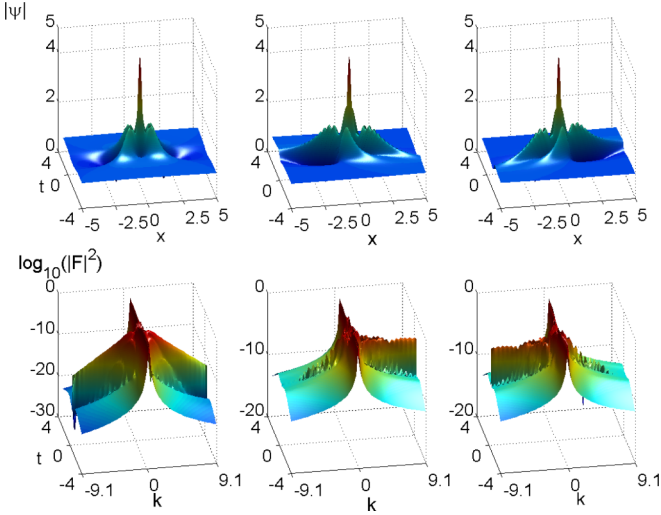


FIG. 4. The top row shows, from left to right, the second-order rogue wave of the KEE for $\beta = 0, 1,$ and $-1,$ respectively, and the bottom row shows the corresponding spectra on a logarithmic scale.

KEE has significantly more widening due to energy acquired by the higher absolute wave numbers compared to its NLSE analog. Even for $t \approx -7,$ the widening of the spectra of the KEE is larger than that of the NLSE. This feature of the KEE spectra may be used to enhance the early detection times of the rogue waves.

We also analyze the second-order rogue wave spectra of the KEE. For the sake of the brevity we do not repeat the exact formulation of the second-order rational soliton solution of the KEE. It is given by Eq. (30) of [8]. We confine ourselves to a presentation of their numerical transforms. Corresponding results are depicted in Figs. 4–6. The results are quite similar to the results obtained for the first-order rogue wave of the KEE, however there are more dips in the spectra due to increased number of zeros in the absolute value of the wave function $|\psi|.$ Similar to the first-order case, the skewness in the second-order

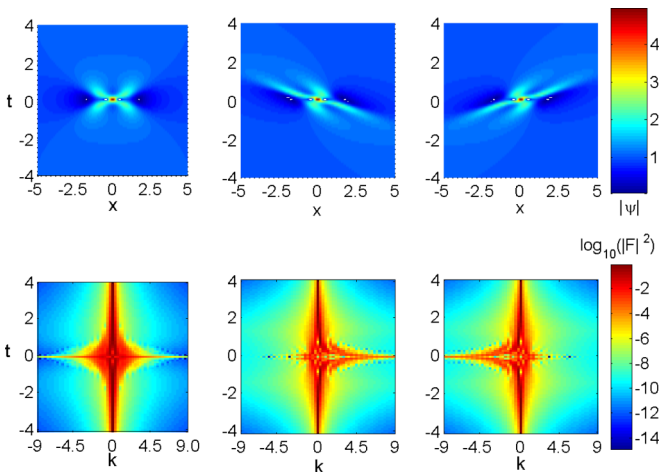


FIG. 5. The top row shows, from left to right, the color contour plot of the second-order rogue wave of the KEE for $\beta = 0, 1,$ and $-1,$ respectively, and the bottom row shows the color contour plot of the corresponding spectra on a logarithmic scale.

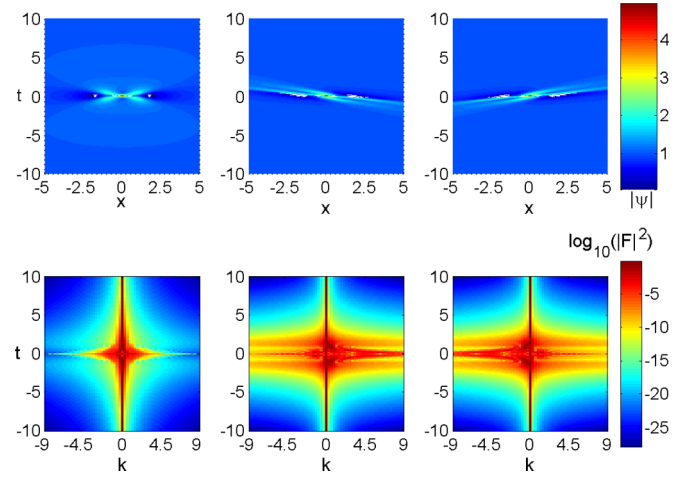


FIG. 6. The top row shows, from left to right, the color contour plot of the second-order rogue wave of the KEE for $\beta = 0, 1.75,$ and $-1.75,$ respectively, and the bottom row shows the color contour plot of the corresponding spectra on a logarithmic scale.

rogue wave field causes a strong asymmetry in the spectra. The triangular widening occurs distinctly on positive wave-number side of the spectrum for the positive values of the β parameter and on the negative wave-number side of the spectrum for the negative values of the β parameter. Similar to the first-order rogue wave case, increasing the skewness in the wave profile results in more asymmetry in the rogue wave spectra, which begin to develop at earlier times of rogue wave emergence compared to their NLSE analogs.

For example, for $t \approx -5,$ there is a significant difference in the widening of the triangular spectra of the second-order rogue wave of the KEE compared to its NLSE analog shown in Fig. 6. For $t \approx -7,$ the difference begins to become significant. Using this feature, the individual rogue waves of the KEE may possibly be detected at earlier stages of their development compared to their NLSE analogs by spectral measurements in practice. This may possibly be done for a wave field under quintic and Raman-effect nonlinear effects. While in an optical setup this may possibly be performed by adjusting the optical properties of the medium, in hydrodynamics a realization would be extremely difficult and only naturally emerging skewed rogue waves may give some clue about the usability of this feature. However, we cannot answer the questions about details of the applicability of this feature in this study. Since a realistic wave field would include many spectral components, we turn our attention to analyze the chaotic wave fields with many spectral components generated in the frame of the KEE by the modulation instability.

III. SPECTRA OF THE CHAOTIC WAVE FIELD

The processes modeled in the frame of the partial differential equations such as the KEE can be very complicated. However, they are still governed by a deterministic equation. Therefore, their results can be predicted for a given initial condition. Therefore, compared to the completely unpredictable stochastic processes, the processes described in the frame of the KEE can be described as chaotic [13]. The term “chaotic”

is used in this setting throughout this paper. We use a numerical framework in order to analyze chaotic wave fields in the frame of the KEE. We start the wave-field simulations using a constant amplitude sinusoid with an additive small-amplitude white noise. Such a state is unstable and it evolves into a full-scale chaotic wave field similar to the wave fields discussed in [2,12,14]. The chaotic wave field modeled by the KEE with this starter evolves into a wave field that exhibits many amplitude peaks, with some of them becoming rogue waves. This behavior is similar to the results obtained for the NLSE and Sasa-Satsuma equation (SSE) [5]. In order to model such a chaotic wave-field starter, we use the initial condition

$$\psi(x, t = 0) = \psi_0(x, 0) + \mu a(x), \quad (5)$$

where $\psi_0 = \exp(ik_0x)$ is the initial plane-wave solution, k_0 is the initial seed plane-wave number, which is selected as $k_0 = 0.1$, and $a(x)$ is a uniformly distributed random complex function with real and imaginary parts having random values in the interval $[-1, 1]$. Following [2,12,14], a value of $\mu = 0.2$ is selected. The water surface fluctuation would be given by the real part of $|\psi| \exp[i\omega t]$, where ω is a carrier wave frequency, however the parameter we investigate is the envelope $|\psi|$ of the chaotic wave field. For the time integration of the KEE, we use the split-step Fourier scheme described in [6]. Briefly, in typical split-step Fourier schemes the spatial derivatives are evaluated using spectral techniques that employ Fourier transforms in periodic domains [15–27] and time stepping is performed by an exponential function. For the sake of brevity, we will not include the details of the split-step scheme of the KEE here. The reader is referred to [6] for a more comprehensive explanation.

Modulation instability is one of the methods used to generate a chaotic wave field [5]. Modulation instability started by the noise formulated above creates a chaotic wave field that starts from the initial plane wave. As recently discussed in [6], the chaotic wave field of the KEE is skewed in the counterclockwise direction for $\beta > 0$ and it is skewed in the clockwise direction for $\beta < 0$, similar to the analytical results. Therefore, the sign of the β parameter controls the skewness direction of the wave field but it does not affect the probability of rogue wave occurrence [6]. Filaments of the chaotic wave field propagate approximately with the average group velocity [6]. Additionally, as the values of the initial seed plane-wave number k_0 gets smaller, the probability of occurrence of extreme waves in the chaotic wave field increases [6]. Similar behavior is also observed for the NLSE and SSE [5], which is possibly an indicator of universal property of the processes started with modulation instability.

In order to demonstrate the possible usage and examine the features of the spectra for the early detection of the rogue waves of the KEE, we choose an area of the chaotic wave field with significantly higher amplitude than other parts. An example of a patch of the chaotic wave field with a rogue wave exceeding amplitude 5 at $t \approx 10.8$ is shown in Fig. 7 in a 3D format. The same chaotic wave field is shown in a contour map format in Fig. 8. A value of $\beta = 1.75$ is used in this simulation and the wave field shown in Fig. 8 is skewed to the left due to positive value of the β parameter, as discussed in [6].

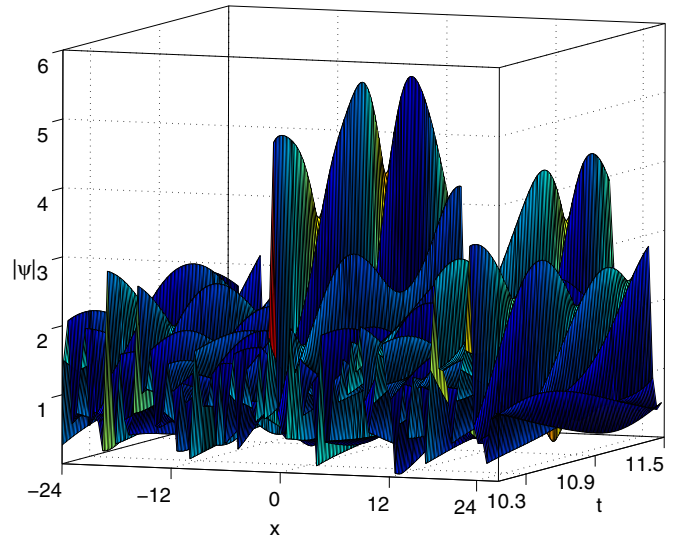


FIG. 7. Example of a rogue wave in the chaotic wave field. The amplitude of this wave exceeds 5.

The spectrum of the chaotic wave field containing the rogue wave is shown in Fig. 9. In order to isolate the features due to the rogue wave in the presence of many spectral components, the spectrum is obtained after a super-Gaussian (Flat-top) mask centered at the location of the peak amplitude is applied to the chaotic wave field. That is, the mask is applied by simple multiplication of the super-Gaussian function with the chaotic wave field that includes the above-mentioned rogue wave in the physical domain. If all of the rogue wave is within the masked zone, then centering of this super-Gaussian function does not affect the spectral results significantly [5].

The spectrum of the patch of the wave field shown in Fig. 9 has a visible widening due to appearance of the rogue wave. A point-by-point comparison of this spectrum with the spectra of the analytical solutions of the KEE presented in the previous sections is extremely difficult. Although some asymmetry in the triangular spectrum with more energy in the

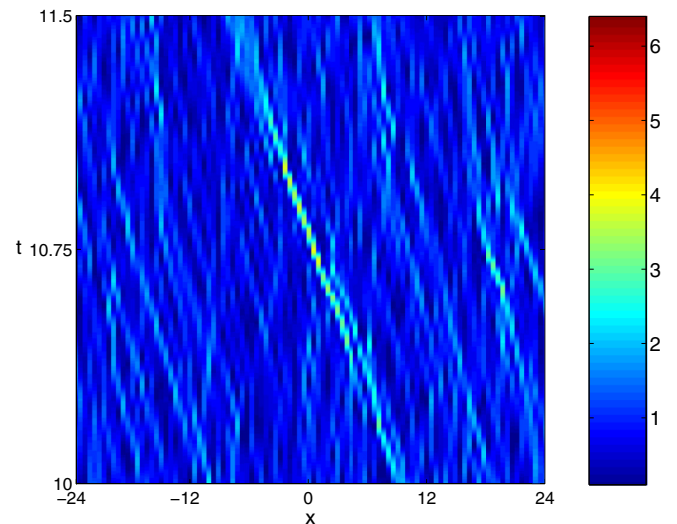


FIG. 8. Contour plot of the rogue wave shown in Fig. 7.

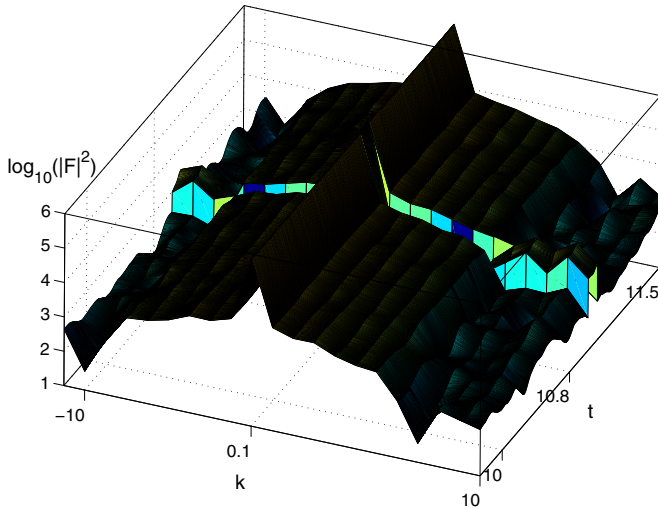


FIG. 9. Spectrum of the chaotic wave field shown in Fig. 7. The apparent widening of the spectrum at $t \approx 10.8$ is due to the appearance of a rogue wave.

positive wave numbers due to the counterclockwise skewness of the wave field that is due to the positive β parameter can be observed, this is not the prominent feature of the spectrum. The prominent feature of the spectrum displayed in Fig. 9 is the considerable widening of the spectrum due to the emergence of the rogue wave. This feature can be used to reveal rogue wave emergence from spectral measurements

[5]. In reality it is only possible to measure a part of the wave field. However, similar to the NLSE and the SSE cases, the spectrum remains triangular even if it is calculated for all or part of the chaotic wave field [5]. This is the main attribute and a universal feature of the typical chaotic wave fields produced through modulation instability [5,28] and characteristic features of the KEE's analytical rogue wave spectra may be suppressed in a realistic chaotic wave field.

IV. CONCLUSION

In this paper we have studied the spectral features of the first- and second-order rational rogue wave solutions of the Kundu-Eckhaus equation. Individual spectra of the rogue waves of the Kundu-Eckhaus equation significantly differ from their NLSE analogs. They exhibit strong asymmetry due to one-sided development of the triangular spectra before the rogue waves become evident in time. As the skewness of the wave field, which is controlled by the β parameter, increases, so does the asymmetry in the triangular spectra. Additionally, the development of the triangular spectra of the rogue waves of the Kundu-Eckhaus equation occurs before their NLSE analogs, which may be used to enhance the early warning times. However, the rogue wave spectra of a chaotic wave field studied in the frame of Kundu-Eckhaus equation have a triangular widening signature similar to the NLSE case as a universal feature of the fields resulting from modulation instability. Therefore, characteristic features of the analytical rogue wave spectra of the Kundu-Eckhaus equation may be suppressed in a realistic chaotic wave field.

-
- [1] N. Akhmediev, A. Ankiewicz, J. M. Soto-Crespo, and J. M. Dudley, *Phys. Lett. A* **375**, 541 (2011).
- [2] C. Bayındır, *Phys. Lett. A* **380**, 156 (2016).
- [3] C. Bayındır, [arXiv:1602.00816](https://arxiv.org/abs/1602.00816).
- [4] J. M. Hollas, *Modern Spectroscopy* (Wiley, New York, 2004).
- [5] N. Akhmediev, J. M. Soto-Crespo, N. Devine, and N. P. Hoffmann, *Physica D* **294**, 37 (2015).
- [6] C. Bayındır, *Phys. Rev. E* **93**, 032201 (2016).
- [7] C. Bayındır, [arXiv:1602.05339](https://arxiv.org/abs/1602.05339).
- [8] X. Wang, B. Yang, Y. Chen, and Y. Yang, *Phys. Scr.* **89**, 095210 (2014).
- [9] L. C. Zhao, C. Liu, and Z. Y. Yang, *Commun. Nonlinear Sci. Num. Simul.* **20**, 9 (2015).
- [10] D. Qiu, J. He, Y. Zhang, and K. Porsezian, *Proc. R. Soc. A* **471**, 0236 (2015).
- [11] B. Oktem, C. Ulgudur, and F. O. Ilday, *Nat. Photon.* **4**, 307 (2010).
- [12] N. Akhmediev, A. Ankiewicz, and J. M. Soto-Crespo, *Phys. Rev. E* **80**, 026601 (2009).
- [13] J. M. Soto-Crespo, N. Devine, N. P. Hoffmann, and N. Akhmediev, *Phys. Rev. E* **90**, 032902 (2014).
- [14] N. Akhmediev, J. M. Soto-Crespo, and A. Ankiewicz, *Phys. Lett. A* **373**, 2137 (2009).
- [15] C. Bayındır, *Sci. Rep.* **6**, 22100 (2016).
- [16] C. Bayındır, M.S. thesis, University of Delaware, 2009.
- [17] E. A. Karjadi, M. Badiy, and J. T. Kirby, *J. Acoust. Soc. Am.* **127**, 1787 (2010).
- [18] E. A. Karjadi, M. Badiy, J. T. Kirby, and C. Bayındır, *IEEE J. Ocean. Eng.* **37**, 112 (2012).
- [19] L. N. Trefethen, *Spectral Methods in MATLAB* (SIAM, Oxford, England, 2000).
- [20] H. Demiray and C. Bayındır, *Phys. Plasmas* **22**, 092105 (2015).
- [21] C. Bayındır, [arXiv:1512.06286](https://arxiv.org/abs/1512.06286).
- [22] C. Bayındır, *J. Appl. Eng. Math.* **5**, 298 (2015).
- [23] C. Bayındır, [arXiv:1512.03584](https://arxiv.org/abs/1512.03584).
- [24] C. Bayındır, [arXiv:1512.03932](https://arxiv.org/abs/1512.03932).
- [25] C. Bayındır, *J. Appl. Eng. Math.* **1**, 135 (2016).
- [26] C. Bayındır, XIX. Türk Mekanik Kongresi, Trabzon, 2015 (unpublished).
- [27] C. Bayındır, Türk Mekanik Kongresi, Trabzon, 2015 (unpublished).
- [28] N. Akhmediev, A. Ankiewicz, J. M. Soto-Crespo, and J. M. Dudley, *Phys. Lett. A* **375**, 775 (2011).